Nonlinear Operation of a MMIC RF Power Amplifier and its Effects on Battery Current, Interference, and Link Margin

Roger A. Dalke
Robert J. Achatz
Yeh Lo

U.S. DEPARTMENT OF COMMERCE
William M. Daley, Secretary

Gregory L. Rohde, Assistant Secretary
for Communications and Information

January 2000

PRODUCT DISCLAIMER

Certain commercial companies, equipment, instruments, and materials are identified in this report to specify adequately the technical aspects of the reported results. In no case does such identification imply recommendation or endorsement by the National Telecommunications and Information Administration, nor does it imply that the material or equipment identified is necessarily the best available for the purpose.

CONTENTS

NONLINEAR OPERATION OF A MMIC RF POWER AMPLIFIER AND ITS EFFECTS ON BATTERY CURRENT, INTERFERENCE, AND LINK MARGIN

Roger A. Dalke, Robert J. Achatz, and Yeh Lo[1]

This report describes measurement, modeling, and simulation methods that are used to analyze the relationship between nonlinear operation of a typical PCS portable transceiver power amplifier and battery current, out-of-band power, and link margin. First the nonlinear characteristics of the PCS amplifier and associated battery current were obtained from amplifier measurements at various bias voltages and RF output signal levels. A mathematical model of the power amplifier based on these measurements was then used to simulate the communications link for purposes of determining the power spectral density and symbol-error ratio for a variable envelope digitally modulated signal using $\pi/4$ DQPSK with 35% root raised cosine filtering. The out-of-band power and symbol-error ratio were computed to determine the link margin for a maximum symbol-error ratio of 10^{-3}.

Key words: MMIC RF power amplifier; PCS transceiver amplifier; nonlinear amplifier; out-of-band power; symbol-error ratio (SER); variable envelope digital modulation; adjacent channel interference

1. INTRODUCTION

Portable transceivers operating in microwave bands are ubiquitous due to the proliferation of 2400-MHz wireless local area network modems, 1900-MHz Personal Communication Services (PCS) phones, 900-MHz PCS two-way pagers, and 800-MHz cellular phones. Each of these devices transmits information over a distance at a specified data rate and reliability while striving to provide the user with acceptable talk- and standby-time. The power amplifier consumes most of the battery current capacity during talk-time and therefore is the main impediment to longer talk-times. One method of increasing talk-time is to use power *efficient* nonlinear amplifiers. For variable envelope modulations, the use of nonlinear amplification distorts the signal, thereby reducing spectral efficiency and reliability. The system designer must balance these competing goals to obtain a reliable power- and spectrum-efficient system.

Power amplifiers are designed so that battery current is conserved whenever possible. For example, during standby-time, battery current is conserved by shutting the power amplifier off. During talk-time, battery current is a function of power amplifier bias voltage and input signal power. In this study we examined the implications of conserving talk-time battery current by varying the bias voltage and input signal power. Specifically, we evaluated the influence of bias voltage and input power on out-of-band power (OBP) and the radio link margin for a typical PCS portable transceiver power amplifier emitting a digitally modulated variable envelope signal.

---
[1] The authors are with the Institute for Telecommunication Sciences, National Telecommunications and Information Administration, U.S. Department of Commerce, Boulder, CO 80303.

When the bias voltage is adjusted to decrease the quiescent current, the nonlinear characteristics of the power amplifier become more pronounced. For variable envelope signals, the corresponding nonlinear transformation of the output current waveform results in distortion of the transmitted signal, ergo undesirable effects such as increased spectrum usage (i.e., OBP) and decreased reliability (i.e., increased symbol errors) must be considered. Increased spectrum usage can also degrade signals in adjacent bands. These effects can be reduced by decreasing or "backing off" the input power; however, this is also undesirable because the corresponding decrease in output power also decreases the link margin.

In this study we evaluated the relationship between battery current, OBP, and link margin by measuring and modeling the nonlinear characteristics of a typical PCS portable transceiver power amplifier at various bias voltages and input signal powers. A nonlinear model of the power amplifier was developed and used to predict the power spectral density (PSD) and required SNR of a π/4 differential quadrature phase-shift keyed (DQPSK) signal filtered by a 35% excess bandwidth root raised cosine (RRC) filter. The OBP was computed from the PSD while the allowable path loss was computed from the output power and required SNR. The approach presented in this paper provides quantitative methods for assessing the electromagnetic compatibility of mobile and fixed link services operating in adjacent bands.

Section 2 describes a typical PCS portable transceiver and explains the relationships between battery current, output power, and link margin. In Section 3, we describe a typical power amplifier and a commonly used circuit model that accounts for the nonlinear behavior of RF power amplifiers. Also, we derive the mathematical model that was used to simulate the *narrowband* portable transceiver described in this report. A description of the amplifier that was measured and modeled along with the measurement configuration and procedures is given in Section 4. The measurement results are summarized in Section 5. In Section 6, we describe the simulation methods used to analyze the amplifier output signal and present the resulting PSD plots and OBP calculations. Section 7 describes the methods used to calculate system performance in terms of symbol-error ratio (SER) as a function of SNR, and gives the results of these calculations. A summary and conclusions are given in Sections 8 and 9.

2. FACTORS AFFECTING PORTABLE TRANSCEIVER BATTERY CURRENT

The portable transceiver considered in this study is typical of those used in cellular radio networks whose base stations are distributed throughout a city, campus, or building. Figure 1 shows a block diagram of such a portable transceiver. The amplified signal passes through a transmit/receive diplexer or switch and a harmonic filter before exciting the antenna.
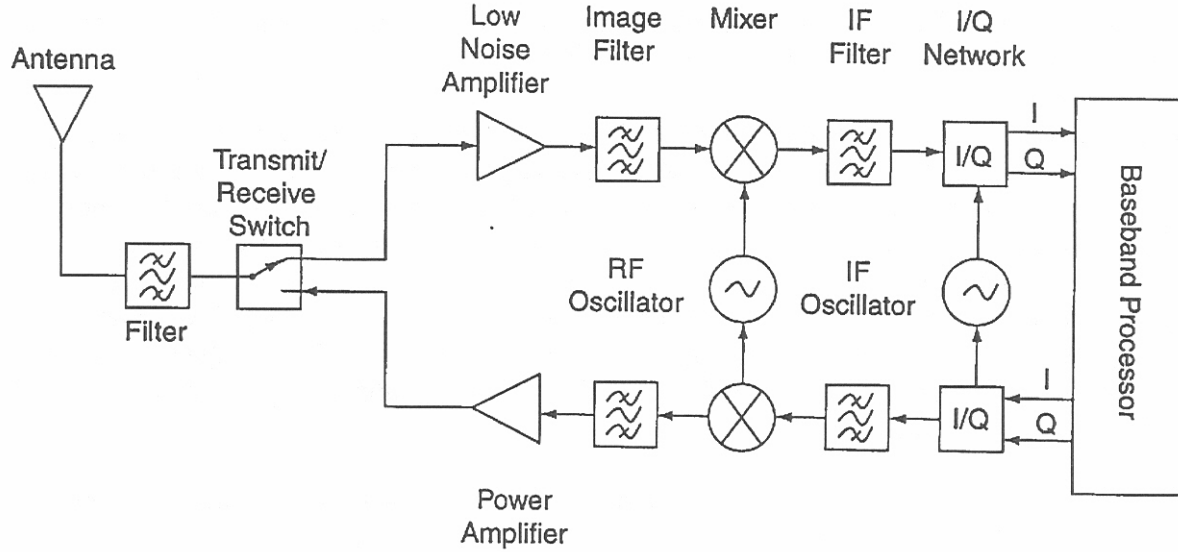
Figure 1. Block diagram of a portable transceiver.

When designing such a communication system, it is essential that the power required to operate the portable transceiver be minimized (i.e., talk-time is maximized). In general, talk-time is a function of the rms battery current I_{DC}, and the battery current capacity C.

$$Talk\text{-}time = \frac{C}{I_{DC}}.$$

The battery current capacity is limited by the battery technology while the battery current is determined by power amplifier operating parameters such as bias voltage and input power. Table 1 shows the battery current capacity of 4 rechargeable 6-V battery packs used to power portable transceivers [1].

Table 1. Voltage and Current Capacity of Portable Transceiver Battery Packs

Electrical Characteristic	Nickel Cadmium	Nickel Metal Hydride	Lithium Ion	Lithium Metal
Voltage (V)	6.0	6.0	7.2	6.0
Current Capacity (A-Hr)	1.0	1.2	0.8	1.6

3

This table shows that talk-time can vary by as much as a factor of 2 for different battery technologies. It should be noted that in addition to battery current capacity, other factors such as cost, volume, and weight are considered in battery selection.

As indicated above, talk-time can be increased by reducing battery current, which is a function of power amplifier operating parameters such as bias voltage and input power. As the bias voltage is decreased, the amplifier becomes *more nonlinear* since the input signal amplitude falls below the transistor's pinch off voltage for a larger portion of an RF carrier cycle. The class of amplifier operation is defined by the percent of time the output current flows in one RF carrier cycle. Class A operation output current flows 100% of the time, Class AB operation output current flows between 50% and 100% of the time, and Class B operation output current flows 50% of the time. Class AB amplifiers are commonly used in portable transceivers where minimizing the power required to operate an amplifier is important [2].

While decreasing bias voltage, in general, reduces the battery current required to operate the amplifier, there are undesirable consequences due to nonlinear amplifier behavior. These nonlinear effects result in an increase in OBP and degradation of system performance. Each of these effects must be carefully analyzed when designing a portable transceiver. In the following sections of this report we analyze these interrelated effects for a typical Class AB PCS RF power amplifier emitting a digitally modulated variable envelope signal.

3. RF POWER AMPLIFIER CHARACTERIZATION

3.1 Typical Portable Transceiver Power Amplifier

A typical multistage power amplifier consists of two or three cascaded amplifier stages with associated bias and matching circuitry. These power amplifiers are made with discrete components mounted on a printed circuit board, microwave integrated circuits (MICS) whose components are integrated into more than one substrate, or as a monolithic microwave integrated circuit (MMIC) whose components are integrated onto a single monolithic substrate [3].

The amplifier stages are made with silicon or GaAs semiconductors. Silicon is used to build either bipolar transistors or metal oxide semiconductor field effect transistors (MOSFET). GaAs is used to build metal epitaxial semiconductor field effect transistors (MESFET). GaAs MESFET's are widely used in portable transceiver power amplifiers because they have a higher frequency range, higher power efficiency, and higher drain to source breakdown voltage than silicon. Figure 2 shows a block diagram of a typical GaAs MESFET multistage power amplifier.
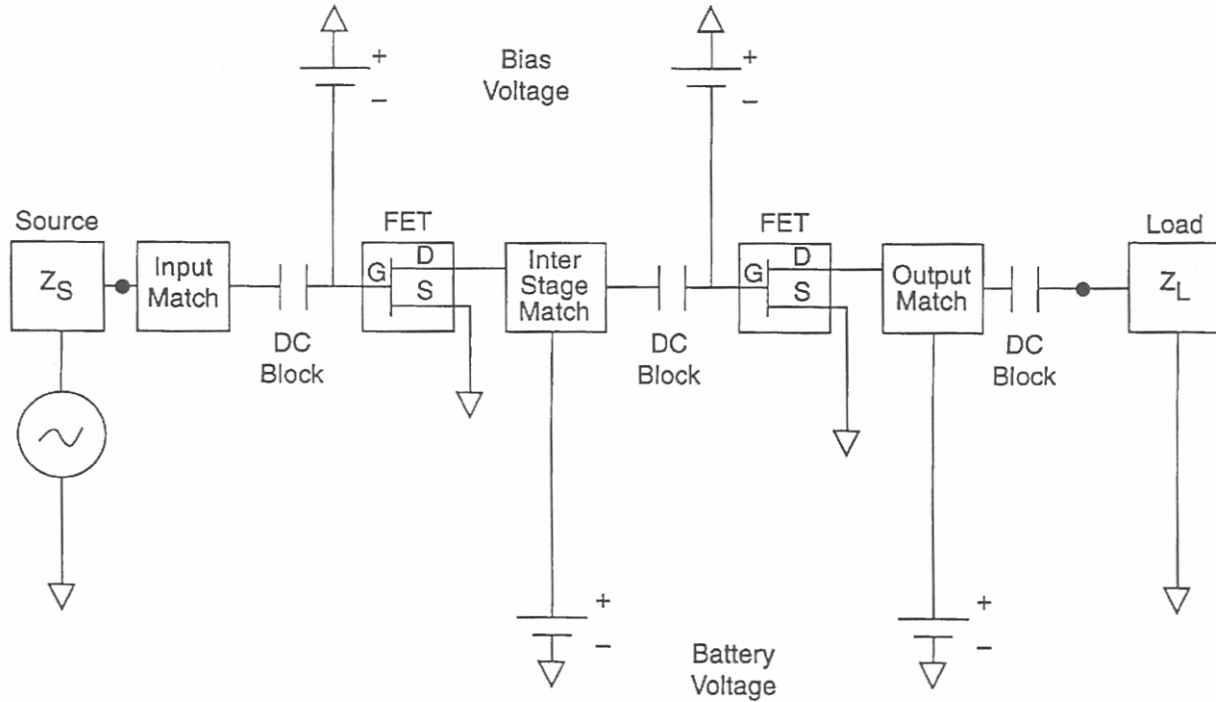
Figure 2. Block diagram of a GaAs multistage power amplifier.

The class of amplifier operation depends upon the bias voltage, input power, battery voltage, and load impedance. In a multistage power amplifier each amplifier stage may have a different class of operation to improve overall power efficiency or linearity. The input matching network impedance is the complex conjugate of the device input impedance for maximum power transfer. Interstage and output matching networks transform input impedance of the next stage to a load resistance that maximizes output power at the fundamental frequency [4, 5]. Harmonic frequencies resulting from nonlinear amplification are commonly shunted to ground.

Table 2 shows the output power required at the antenna input for some typical portable transceiver applications [6]. Power amplifier output power is found by adding 1-2 dB to these values to compensate for the losses between the power amplifier output and the antenna.

Table 2. Typical Output Power Used in Portable Transceiver Applications

Portable Transceiver Application	Output power (dBm)
2400-MHz WLAN modem	20.0
1900-MHz TAG-5 DCS-based TDMA PCS phone	30.0
1900-MHz TAG-4 IS-136-based TDMA PCS phone	27.8
1900-MHz TAG-2 CDMA PCS phone	23.0
1900-MHz TAG-3 TDMA PCS phone	20.0
900-MHz PCS two-way paging	30.0
800-MHz cellular phone	27.8

Figure 3 depicts the location of the gate, drain, and source components of a typical GaAS MESFET integrated onto a substrate [7]. Figure 4 illustrates the (large signal) equivalent circuit of the same GaAS MESFET [8]. R_S, R_D, R_G, and L_S, L_D, L_G are the parasitic resistances and inductances for the source, drain, and gate respectively. C_{DS} is the drain-to-source capacitance. C_G and C_D are the gate--to-channel capacitances while R_i is the gate-to-channel resistance. I_D is the internal drain current source. The most significant sources of nonlinear behavior are C_G, C_D, and I_D. Each is a function of V_G and V_D as shown in Figure 4.
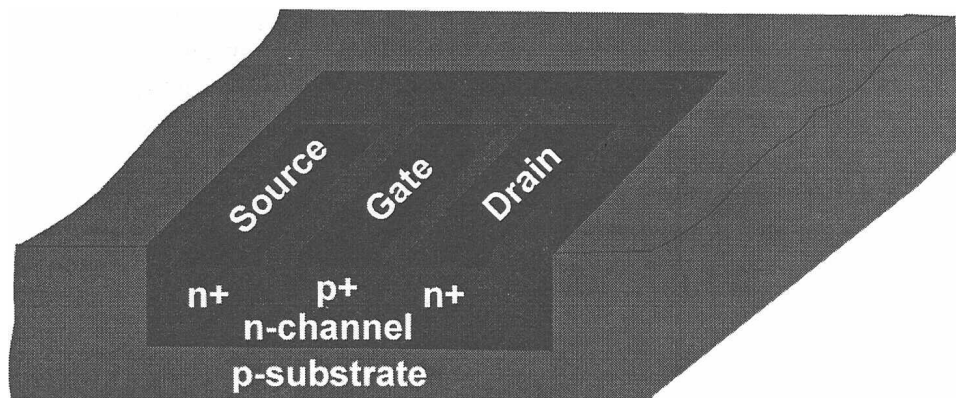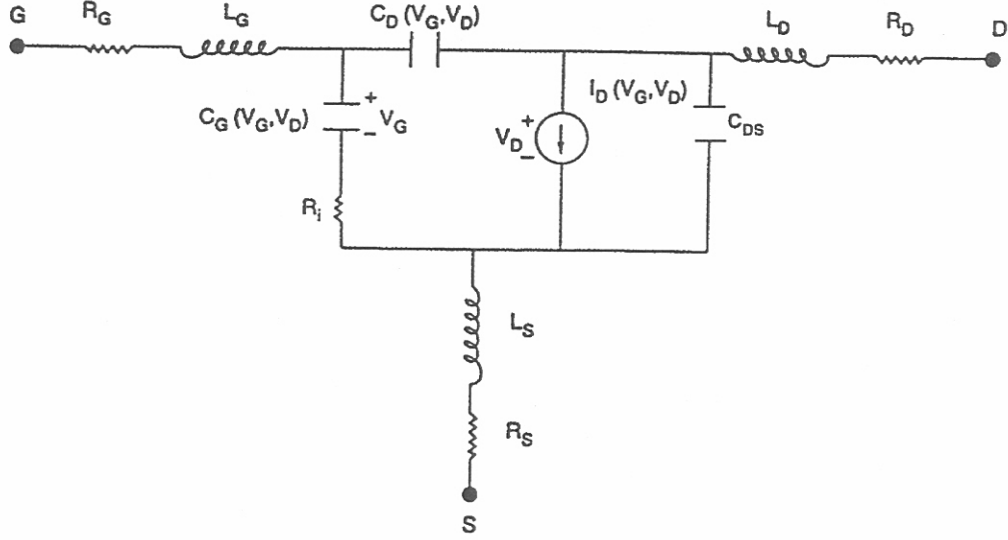

Figure 3. Integrated GaAS MESFET.

Figure 4. Equivalent circuit of GaAs MESFET.

3.2 A General Mathematical Model for Nonlinear Narrowband RF Power Amplifiers

In this subsection we derive a mathematical model that characterizes a narrowband nonlinear power amplifier. The primary purpose of what follows is to show that this particular model is valid for a fairly general class of narrowband nonlinear systems. Essentially the amplifier is treated as a generic nonlinear system that operates on a *narrowband* RF input such as may be used in a digital communications system. It is shown that for a sufficiently narrow bandwidth, the nonlinear amplifier can be characterized by two functions of the input signal envelope voltage. These functions can be determined empirically from direct measurements of the amplifier or from the analysis of amplifier circuit models such as that shown in Figure 4. This model is commonly used for the analysis of narrowband nonlinear power amplifiers [9].

Suppose we have an electronic device where the output y_0 at a particular time t depends in a nonlinear way on the input x_0 at all times prior to t or $x_0(t-\xi)$ for all ξ, $\xi \geq 0$. The input can be considered as a function of ξ and a parameter t, i.e. $u(\xi;t)$. Assuming that the system is stationary, $u(\xi) \in L^2$ (i.e., u is square-integrable), and $y_0(t) \in L^2$, then we can write the nonlinear response in terms of a functional series [10]

$$y_0(t) = G[u(\xi;t)] = \sum_{n=0}^{\infty} \frac{1}{n!} F_n[u(\xi;t)],$$

(3-1)

7

where $F_n[u]$ is a regular homogenous functional of the form

$$F_n[u(\xi;t)] = \int_{-\infty}^{\infty} ... \int_{-\infty}^{\infty} k_n(\xi_1,...,\xi_n)u(\xi_1;t)...u(\xi_n;t)d\xi_1...d\xi_n \tag{3-2}$$

and where the kernel functions $k_n(\xi_1,...,\xi_n) \in L^2$ are symmetric with respect to their arguments (ξ_n) as defined in [11]. The kernel functions are determined independently of the variable function u. If the function $u(\xi;t)$ is an analytic function of t then the functional $G[u(\xi;t)]=y_0(t)$ is also an analytic function of t.

The *Volterra Series* [12] given by Equation 3-1 is applicable to a substantial number of electronic systems encountered in communication problems and is commonly used to calculate distortion in various types of amplifiers. For our purposes it is assumed that the input signal to such a device has the form

$$x_0(t) = \text{Re}\{xe^{-i2\pi ft}\} = A\cos(2\pi ft - \psi) \tag{3-3}$$

where the complex amplitude is $x = A\,e^{i\psi}$ and x (and hence both A and ψ) might vary with time so as to modulate a carrier at the frequency f. If the variation is slow, we will assume that a steady-state analysis is appropriate for our purposes.

For this harmonic input, we have [11]

$$y_0(t) = \sum_{n=1}^{\infty} \sum_{k=0}^{\infty} \left(\frac{A}{2}\right)^n \frac{e^{(-i2\pi f + i\psi)(2k-n)}}{k!(n-k)!} K_{k,n-k}(f) \tag{3-4}$$

where

$$K_{k,n-k}(f) = K_n(f_1,...f_k, f_{k+1},...,f_n)$$

$$f_m = \begin{cases} f & m \le k \\ -f & k+1 \le m \le n \end{cases} \tag{3-5}$$

and $K_n(f_1,...,f_n)$ is the n-fold Fourier transform of $k_n(\xi_1,...,\xi_n)$.

The system response is required to be a causal real function of time, hence

$$K_n(f_1,...,f_n) = K_n^*(-f_1,...,-f_n) \tag{3-6}$$

8

where the asterisk superscript denotes the complex conjugate. In addition, if $h(t)$ is the system response then causality requires that

$$h(t) = s(t)\, h(t) \tag{3-8}$$

where $s(t)$ is the unit step function. If the Fourier transform of the system response is $H(f)$, the causality requirement can be written as

$$H(f) = \frac{1}{2}\left[H(f) + \frac{1}{i\pi} \wp \int_{-\infty}^{\infty} \frac{H(x)}{f-x}\, dx \right]. \tag{3-9}$$

Hence, the real and imaginary parts of the Fourier transform form a Hilbert transform pair, explicitly

$$\Re\{H(f)\} = \frac{1}{\pi} \wp \int_{-\infty}^{\infty} \frac{\Im\{H(x)\}}{f-x}\, dx$$

$$\Im\{H(f)\} = -\frac{1}{\pi} \wp \int_{-\infty}^{\infty} \frac{\Re\{H(x)\}}{f-x}\, dx \tag{3-10}$$

where $\wp$ denotes the principal value of the integral, $\Im$ the imaginary part of the function, and $\Re$ the real part of the function.

For a narrowband power amplifier, the harmonics are suppressed resulting in the series:

$$y(t) = e^{-i2\pi ft + i\psi}\left[\frac{A}{2} K_1(f) + \frac{A^3}{16} K_3(f,f,-f) + \dots \right]$$

$$+ e^{i2\pi ft - i\psi}\left[\frac{A}{2} K_1^*(f) + \frac{A^3}{16} K_3^*(f,f,-f) + \dots \right], \tag{3-11}$$

which is a real function of time as required. From the causality requirement, in general, the functions $K_n(\bullet)$ are complex. For a single frequency we have a series of complex numbers scaled by increasing powers of the input signal amplitude that can be written in polar form where clearly both the output amplitude and phase are functions of the input amplitude A

$$y(t) = \Re\left\{ e^{-i2\pi ft + i\psi} \sum_{n=1}^{\infty} A^n z_n \right\} = \Re\left\{ e^{-i2\pi ft + i\psi} \rho(A) e^{i\phi(A)} \right\} \tag{3-12}$$

9

This expression leads directly to a fairly general characterization of the baseband transfer function for a narrowband nonlinear power amplifier

$$\hat{y}(t) = \rho(A)e^{i\phi(A)-i\psi} = \frac{\rho(A)}{A}e^{i\phi(A)}x = g(A)x \qquad (3\text{-}13)$$

where $g(A)$ is the complex gain function. It is interesting to note that when the $K_n(\bullet)$ are pure real, the system is memoryless and the output only depends on the present value of the input (i.e., the $k_n(\bullet)$ are weighted Dirac delta functions). It should also be recalled that when Equation 3-12 is used to analyze communications devices, it is assumed that the bandwidth is sufficiently narrow that the steady-state approximation is reasonable.

3.3 Determination of AM-AM and AM-PM Characteristics for a Narrowband Portable Transceiver Power Amplifier

The previous analysis shows that two functions are required to characterize the output of a narrowband nonlinear power amplifier. The function $\rho(A)$ describes the *amplitude-pushing* characteristics (AM-AM) of the device. The function $\varphi(A)$ describes the *phase-pushing* characteristics (AM-PM) of the device. Once these functions are determined, Equation 3-12 can be used to simulate the signal emitted by a portable transceiver power amplifier. The output of such a simulation can be used to calculate the power spectral density or SER for an amplified digitally modulated variable envelope signal. The results of such an analysis are given in Sections 6 and 7.

In general, the nonlinear functions can be determined either by creating and analyzing a device model (e.g., an equivalent circuit) or direct RF measurements. Nonlinearities of field effect transistors commonly used in power amplifiers can be accounted for in equivalent circuit models by introducing appropriate variations in the circuit elements as functions of instantaneous drain and gate voltages such as that shown in Figure 4. For our purposes, the two nonlinear functions were obtained from RF measurements described in the following section.

4. RF POWER AMPLIFIER MEASUREMENT DESCRIPTION

4.1 Test Fixture

A power amplifier targeted for portable transceivers transmitting in the 2-GHz PCS band was used to evaluate the relationship between battery current, OBP, and link margin for a commercially available power amplifier. The nonlinear characteristics of this particular amplifier were determined from the measurements described in this section. The nonlinear model developed from these measurements was then used in simulations to obtain PSD and SER curves as described in the following sections.

The power amplifier contains three amplifier stages in a 16-pin case. It has a maximum gain in excess of 30 dB and can transmit more than 2 W of power. It is mounted on a printed circuit board with a power amplifier support integrated circuit (IC), drain current control, input and output matching networks, and bias voltage divider network. The test fixture is powered by an adjustable power supply set to 4.8 V capable of supplying 3 A of drain current. A block diagram of the test fixture is shown in Figure 5.

The drain current controller is used to conserve battery current when not transmitting. In our tests the V_{RAMP} and V_{IDLE} pins of the power amplifier support IC were set so that drain current control was disabled. This forced the power amplifier to operate continuously at a power level determined by the bias voltage and input power. Additional heat sinking was added to insure that the power amplifier did not overheat. Input, interstage, and output matching was tuned for the 1850- to 1910-MHz band. The test fixture had 50 Ω input and output impedance that matched interfacing RF test equipment.

The biasing of all three amplifier stages was controlled by a common pin on the case; thus variation of individual amplifier stage bias voltages was not possible. Bias voltage control was adjustable, as shown in Figure 5. The power amplifier support IC generated -4.0 V for the bias voltage. An adjustable voltage divider was used to vary the bias voltage to any value from -4.0 to 0 V. The lower voltage corresponded to a negligible quiescent current, whereas the higher voltage corresponded to a relatively large quiescent current.
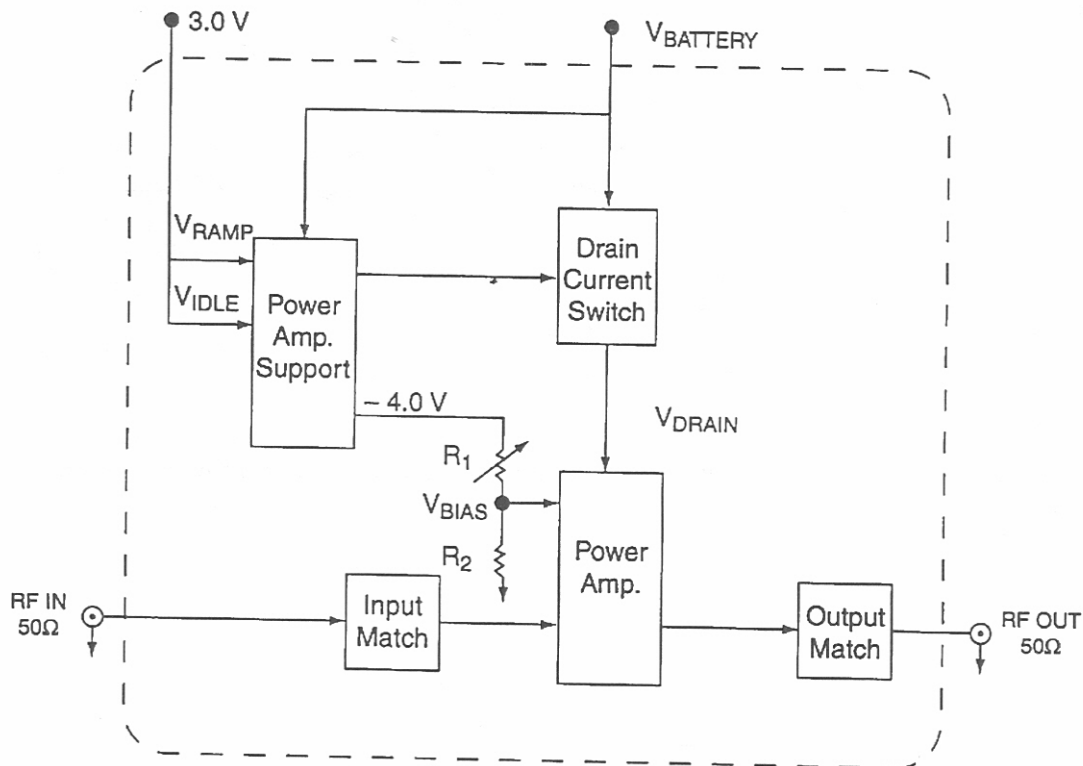

Figure 5. Block diagram of power amplifier test fixture.

4.2 Amplitude and Phase Measurement

The AM-AM and AM-PM measurements were obtained with the equipment depicted in Figure 6. The continuous wave signal out of the signal generator was amplified and split into test and reference channels. The test channel was power amplified by the test fixture whereas the reference channel was not. A spectrum analyzer was used to measure the amplitude of the test channel for the AM-AM function. The phase measurement circuit, shown in Figure 7, was used to measure the phase difference between the test and reference signals for the AM-PM function. Battery current was measured with an ammeter placed between the adjustable power supply and the test fixture as shown in Figure 6. The current measurements included all power normally required to operate the power amplifier. This included the relatively small currents required for the power amplifier support IC and drain current control.
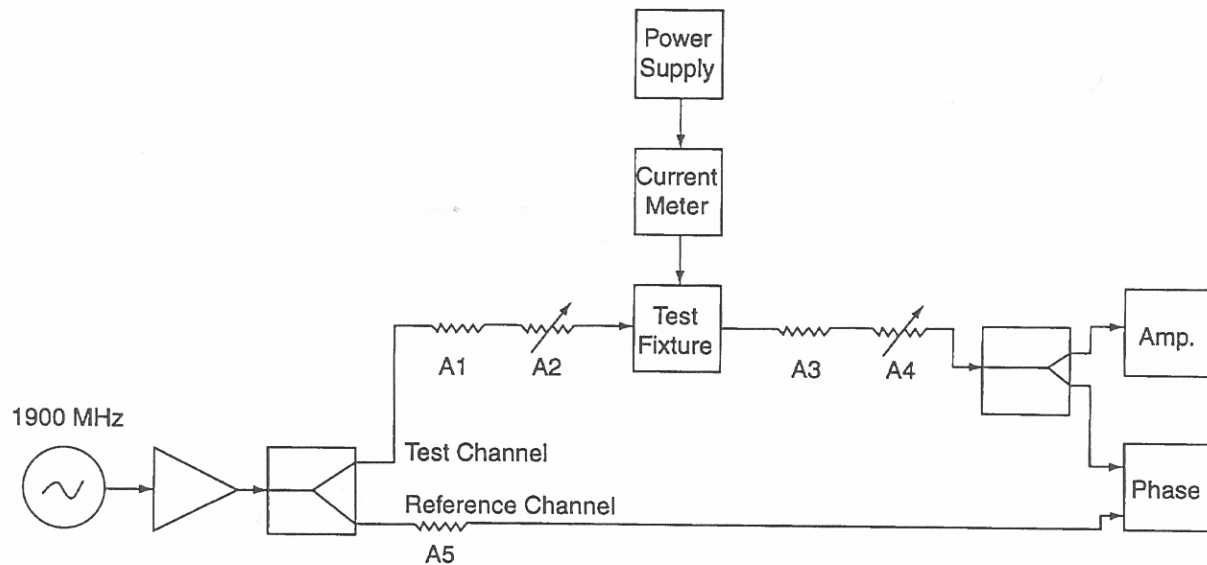

Figure 6. Block diagram of AM-AM, AM-PM, and battery current measurement setup.
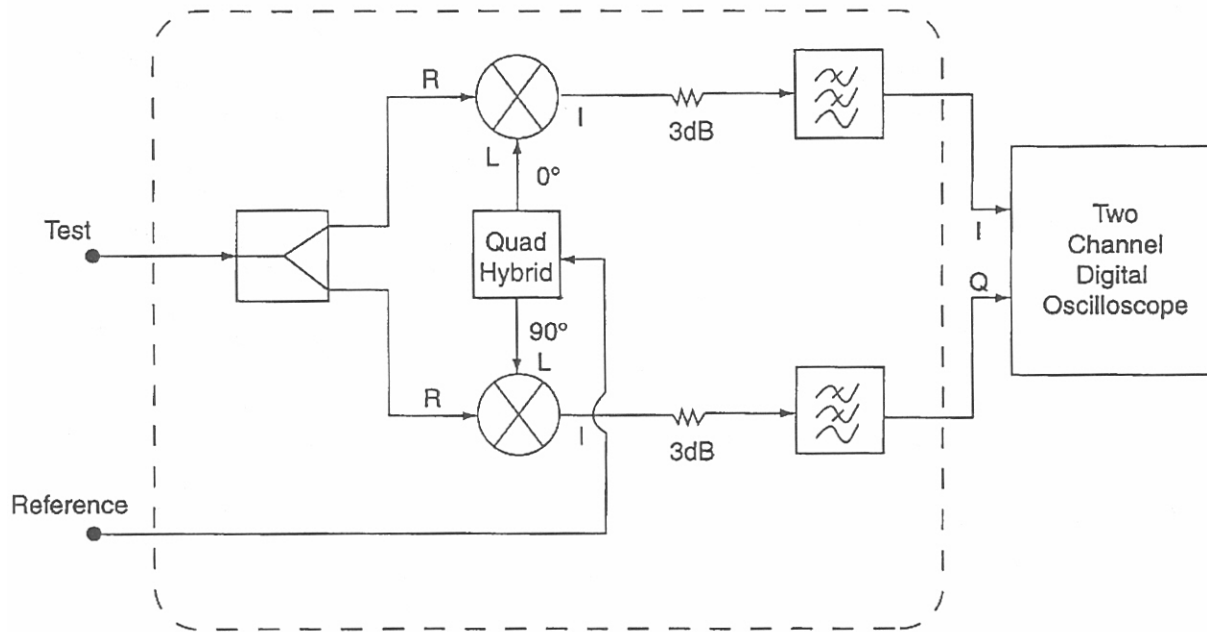
Figure 7. Block diagram of phase measurement setup.

5. RF POWER AMPLIFIER MEASUREMENT RESULTS

In this section we present the results of the RF power amplifier measurements described in Section 4. Measurements of the narrowband nonlinear functions (i.e., AM-AM and AM-PM) and associated power supply current were acquired for various bias voltages. The results presented in this section are for bias voltages of -2 V, -2.25 V, and -2.5 V.

5.1 AM-AM and AM-PM Measurements

Least-square fitting routines were used to fit rational functions to the measured AM-AM and AM-PM data. Typically, the data were divided into sections and fit with low-order polynomials or rational functions. These functions were used to characterize the nonlinear amplifier behavior in the simulations described in Sections 6 and 7. The measured data and approximations are given in the Appendix.

Figure 8 shows the curves that were fit to the measured AM-AM and AM-PM functions for the various bias voltages. Figure 9 shows the gain as a function of the input power. It should be noted that as the bias voltage decreases, the gain decreases and significant nonlinear behavior occurs at relatively larger inputs.
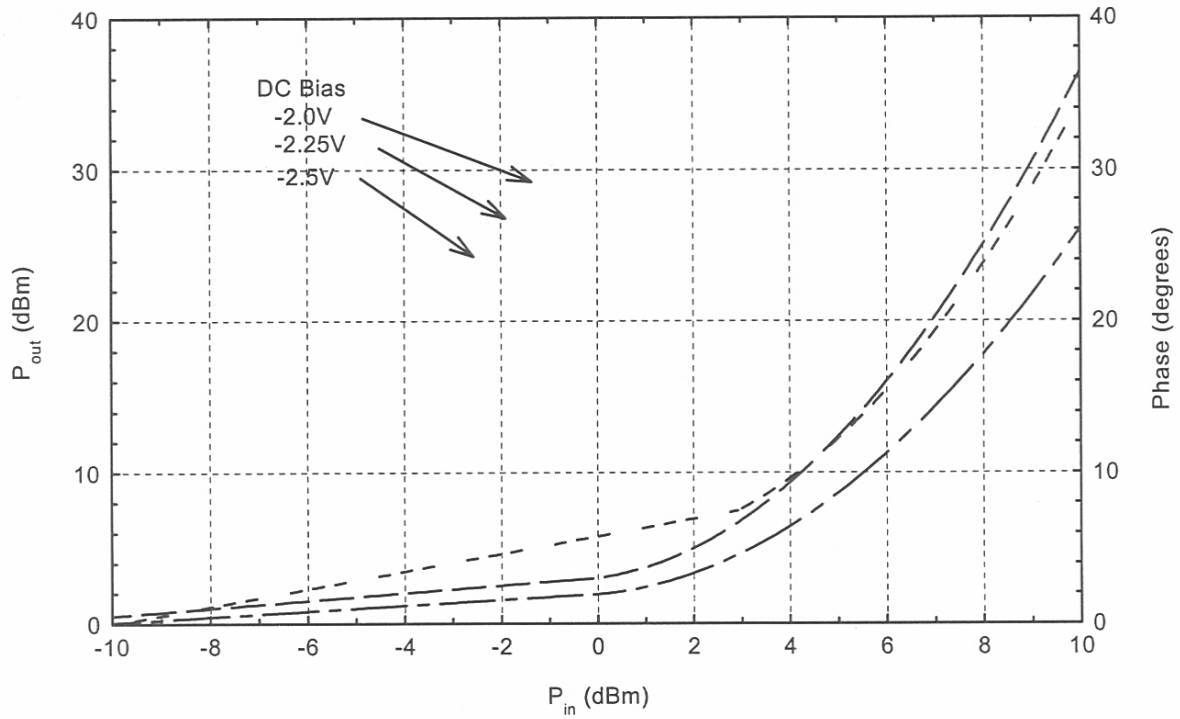
13

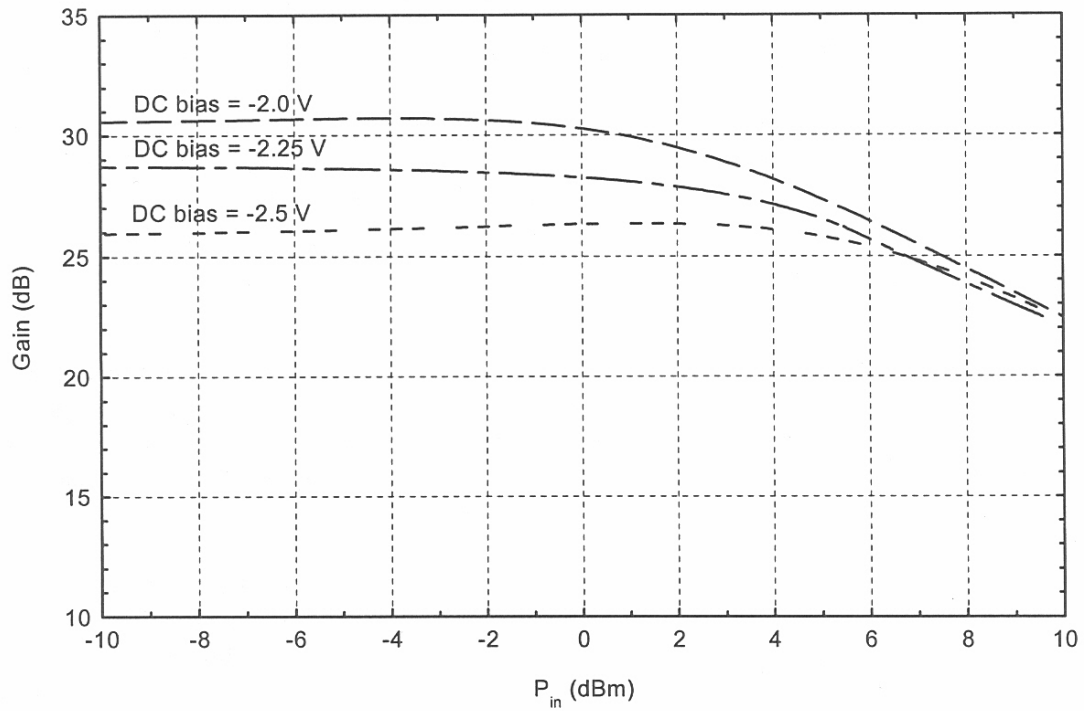Figure 8. AM-AM and AM-PM for three bias voltages.

Figure 9. Gain for three bias voltages.

14

5.2 Power Supply Current and Efficiency

The measured average power supply current for bias voltages of -2.0 V, -2.25 V, and -2.5 V are shown in Figure 10 as a function of the input power P_{in}. Note that the power supply current increases (nonlinearly) as both P_{in} and bias voltage increase. Clearly, reducing the bias voltage for a fixed P_{in} reduces the required power supply current. As indicated in Figure 9, decreasing the bias voltage for a fixed P_{in} also decreases the power gain. Hence, to maintain a fixed output power, P_{in} must be increased when bias voltage is decreased. If a significant increase in P_{in} is required, the savings in power supply current may be fairly small, as noted in Figure 10, for bias levels of -2.0 V and -2.25 V.
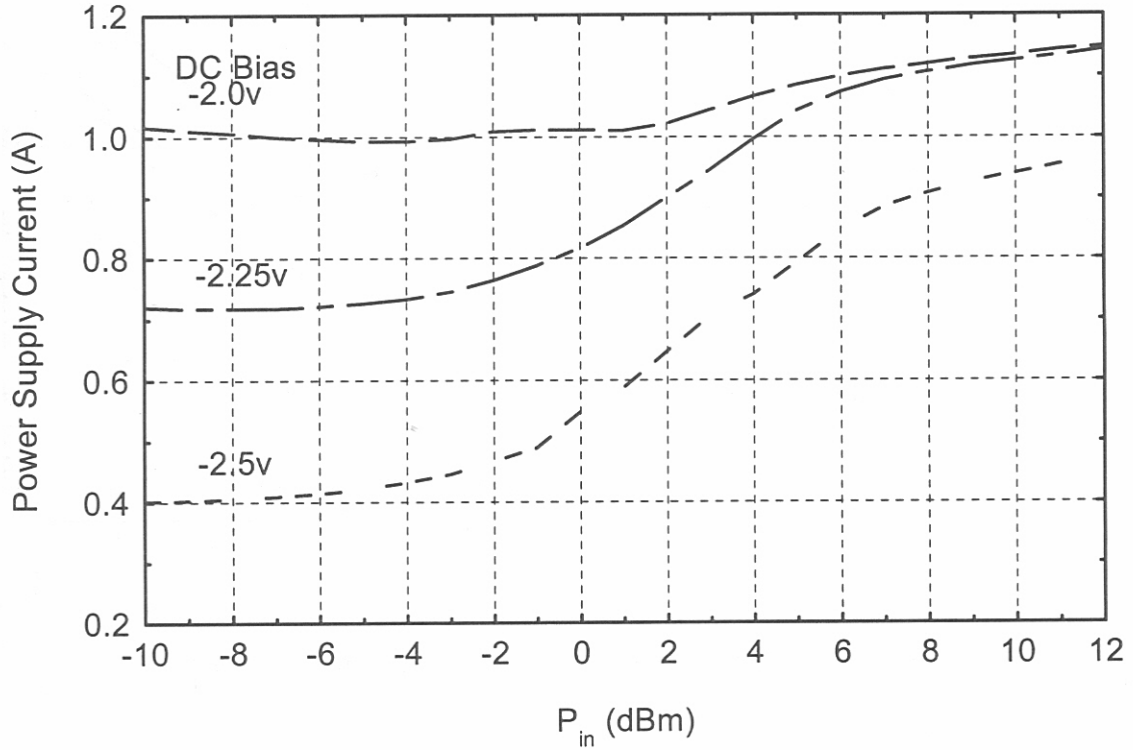

Figure 10. Power supply current for three bias voltages.

Two related power amplifier quantities of interest in communications engineering are the output power P_{out} and the power supply current. In general, P_{out} must be sufficient to yield the minimum SER for a given communications link and signal modulation. A commonly used measure that relates the power supply voltage and current and P_{out} for power amplifiers is the *power-added* efficiency, defined as

$$\eta = \frac{P_{out} - P_{in}}{V_{DC}I_{DC}}.$$

where V_{DC} and I_{DC} are the power supply voltage and current.

15

In Figure 11 we have plotted η as a function of P_{out} for the three bias voltages. It is clear from this figure that for an output power of less than 31 dBm, decreasing the bias voltage increases the efficiency (i.e., decreases the power supply current). Of course merely decreasing the bias to decrease power supply current may not be appropriate since decreasing the bias voltage will result in increased signal distortion that can have a deleterious effect on the OBP and SER (as will be shown in Sections 6 and 7).
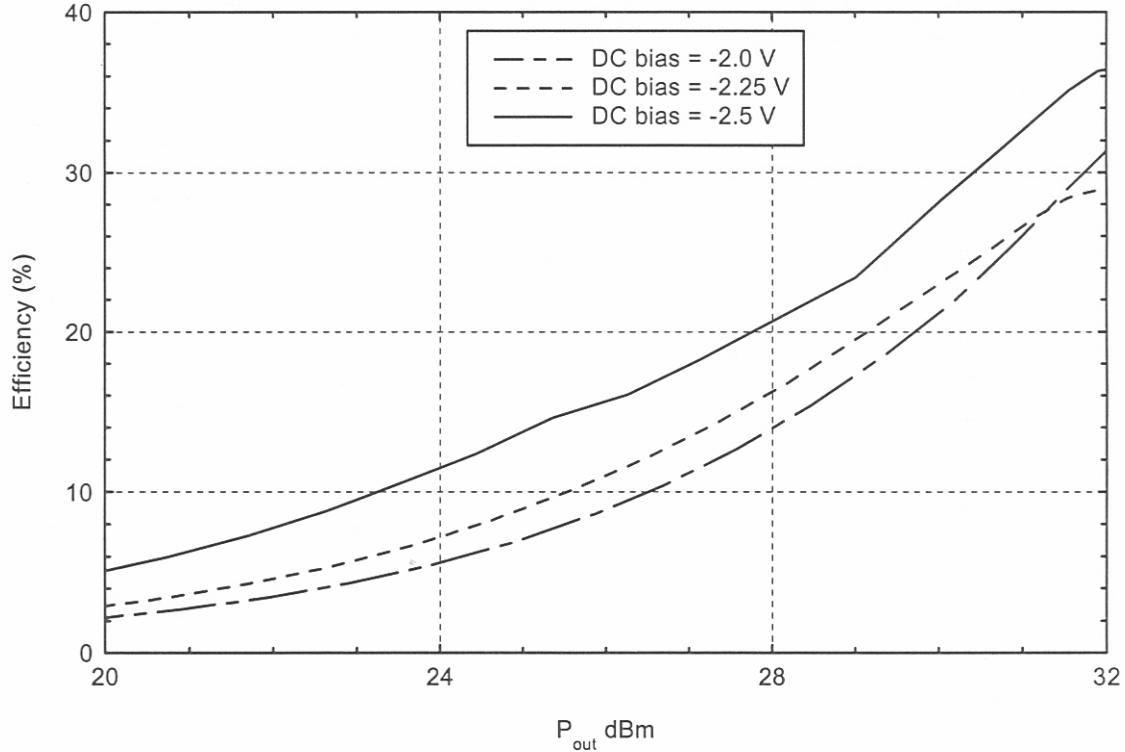

Figure 11. Power-added efficiency for three bias voltages.

6. REQUIRED SIGNAL-TO-NOISE RATIO AND LINK MARGIN FOR π/4 DQPSK

The reliability of a radio link can be measured by the symbol error rate (SER). In this study, the radio link SER is determined using simulation methods. The simulated link corresponds to the physical channel defined by the cellular and PCS IS 136/54 mobile radio standard. The standard uses π/4 differential quadrature phase-shift keying (DQPSK) modulation filtered with a 35% excess bandwidth root raised cosine (RRC) pulse-shaping filter. The transmission rate is 24,300 symbols/s or 48,600 bits/s and the channel spacing is 30 kHz. Multiple access and duplexing features of IS 136/54 were omitted.

A block diagram of the transmitter and receiver used in the simulation is shown in Figure 12. A uniform random number generator produces a random sequence of 2-bit symbols to be transmitted. These symbols are mapped to their corresponding QPSK symbols. The differential encoder adds the

phase of the current symbol to the sum of the phases of all preceding symbols. The symbols are then up-sampled to 16 samples/symbol (N-1 zeros are appended to the sequence after each symbol where N is the number of samples per symbol) and filtered by a finite impulse response RRC pulse-shaping filter to yield the digitally modulated signal.

The amplifier model, based on the narrowband nonlinear model derived in Section 3 and using the nonlinear functions described in Section 5, multiplies the undistorted digitally modulated signal by a complex gain that is a function of signal amplitude. The normalized complex gain (see Equation 3-13) is computed as follows:

$$g_0(t) = \frac{g(A(t))}{g(A_{op})},$$

where $A^2(t)$ is the instantaneous input signal power and A_{op}^2 is the mean input signal power.
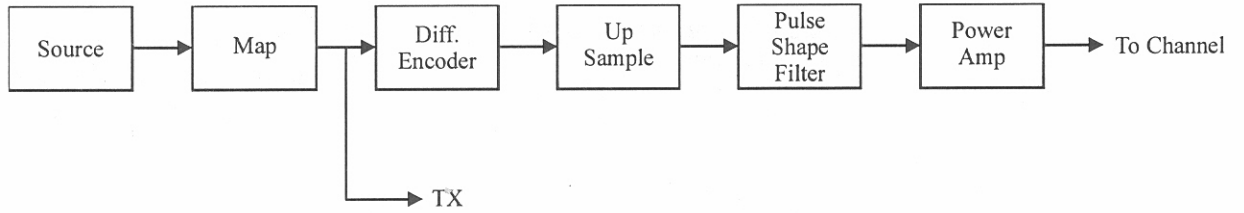

Figure 12a. Block diagram of simulated $\pi/4$ DQPSK with RRC filtering transmitter.
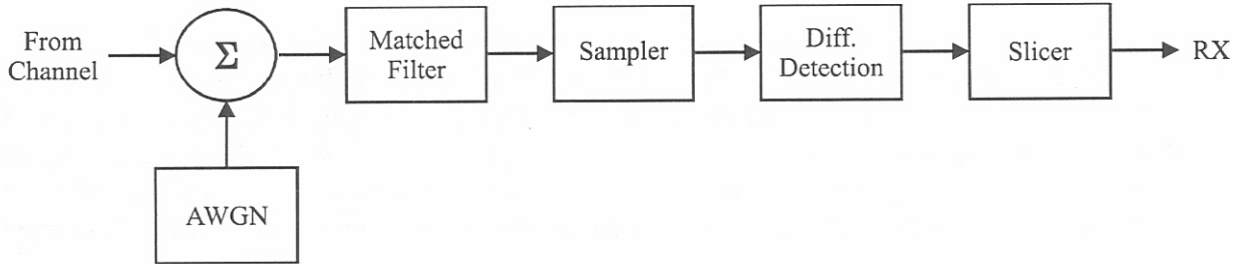
Figure 12b. Block diagram of simulated $\pi/4$ DQPSK with RRC filtering receiver.

White Gaussian noise was added prior to the receiver's RRC matched filter. The output of the matched filter was sampled once per symbol. The symbols were detected by subtracting the phase of the previous symbol from the present one. The decision block (slicer) decided which symbol was sent. This symbol was compared to the transmitted symbol to determine the number of received symbol errors.

17

Figure 13 shows the SER curves for P_{out} = 28 and 31 dBm in combination with biases of -2.0 and -2.5 V, respectively, compared to the theoretical performance for a linear amplifier. These results correspond to the *most* linear and the *worst-case* nonlinear operation of the amplifier based on the measurements presented in this report. Figure 13 contains error bars corresponding to a standard deviation in computed SER.
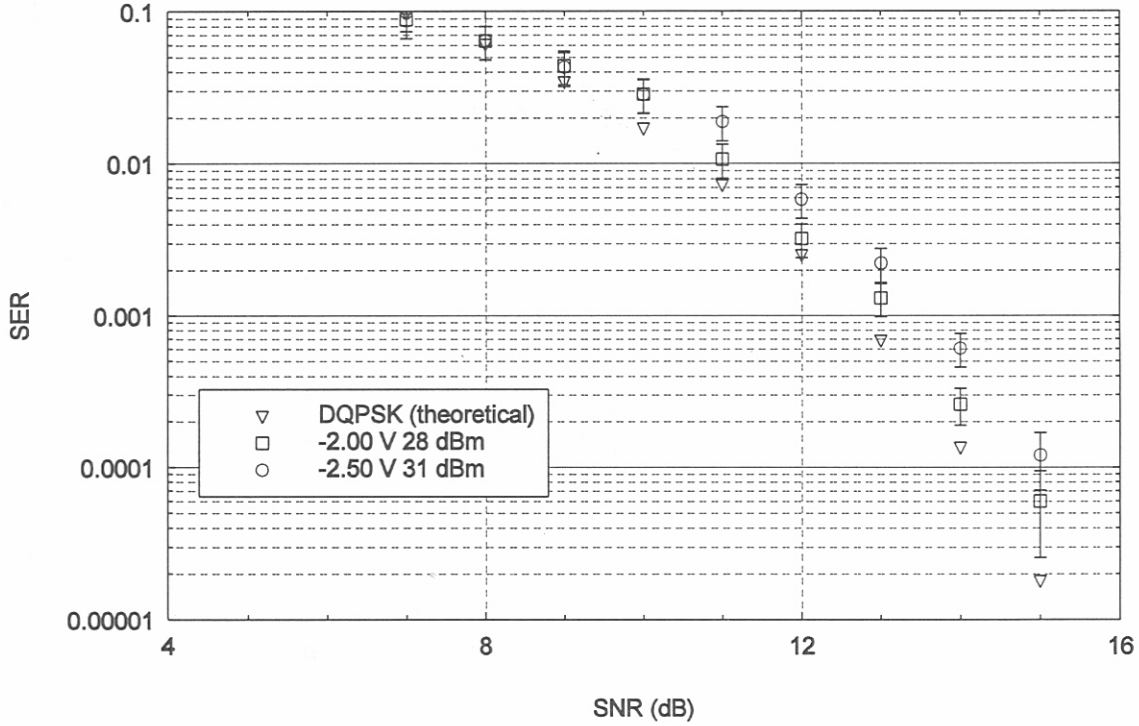

Figure 13. SER in an AWGN channel for a portable transceiver communications link.

The received signal power is a function of the radio link loss; this along with effective isotropic radiated power and required SER (and hence SNR) determines the link margin of the transceiver. In order to compare the results for various amplifier operating conditions, the link margin for the transceiver operating at the 3 bias voltages and P_{out} = 28, 29, 30, and 31 dBm were calculated relative to a reference link margin where the transceiver is operated at P_{out} = 28 dBm and -2.0 V bias. When the propagation path is assumed to be the same for all cases, the relative link margin (RLM) is given by:

$$RLM = P_{out} - SNR_{req} - [P_{out} - SNR_{req}]_{reference} \ (dB)$$

where SNR_{req} is that required to achieve an SER of 10^{-3}. Assuming the reference link margin is the desired link margin, the additional power given by the RLM corresponds to an allowable increase in effective range over the reference case. For example assuming only free space loss, each additional 6 dB in RLM corresponds to doubling the effective range relative to the reference case.

Table 3 shows the SNR and RLM for each of the cases described above. The required SNR for a linearly amplified signal is 12.9 dB which for each output power would increase the RLM by a fraction of a dB. Assuming only free space loss, the 2.9 dB RLM at P_{out} =31 dBm and -2.0 V P_{out} corresponds to an increase in effective range of about 40%.

Table 3. Required SNR and RLM as a Function of Bias Voltage and Output Power

P_{out}	Bias (V)	SNR @ 10^{-3} SER (dB)	RLM (dB)
31 dBm	-2.50	13.6	2.6
	-2.25	13.6	2.6
	-2.00	13.3	2.9
30 dBm	-2.50	13.1	2.1
	-2.25	13.2	2.0
	-2.00	13.1	2.1
29 dBm	-2.50	13.1	1.1
	-2.25	13.1	1.1
	-2.00	13.2	1.0
28 dBm	-2.50	13.1	0.1
	-2.25	13.1	0.1
	-2.00	13.2	0.0

7. POWER SPECTRAL DENSITY FOR π/4 DQPSK

The spectral efficiency of a communication system using a variable envelope modulation scheme depends on the symbol rate, the transmitter filter, and the nonlinear characteristics of the power amplifier. In this section, we give estimates of the PSD for a radio link that utilizes a digitally modulated signal based on the IS 136/54 standard described in Section 6. The PSD was calculated using simulation methods incorporating the *narrowband* nonlinear models from Section 3.

Baseband digital simulation of the amplified signal was accomplished by creating a filtered π/4 DQPSK symbol stream digitized with 13 samples per symbol and applying the nonlinear functions that represent the power amplifier behavior. The filtered symbol stream (weighted impulses) was generated using a pseudorandom noise code that was convolved with a finite impulse response filter based on the RRC pulse shape. The PSD of the *distorted transmitted* signal was obtained by using the Welsch method for averaging modified periodograms [13]. In this method, a Hanning window is applied to a simulated output data segment consisting of 4096 samples. The PSD was estimated by performing a Fourier transform of each data segment and averaging the square of the magnitude of several hundred transformed data segments.

Figures 14-17 show the calculated normalized PSD's for output powers of 28, 29, 30, and 31 dBm; bias voltages of -2.0 V, -2.25 V, and -2.5 V; and 24,300 symbols/s (30 kHz channel spacing). The OBP for each case is given in Table 4 below. For the purposes of this report, OBP is the ratio of power contained outside of a specified channel to the total power and is obtained by integrating the PSD as follows:

$$W_c = \int_{-B/2}^{B/2} S(f)df, \quad W_T = \int_{-\infty}^{\infty} S(f)df$$

$$OBP = 1 - \frac{W_c}{W_T}$$

where S (f) is the power spectral density and B is the channel spacing.

Figures 14-17 show that for a fixed P_{out}, the OBP increases with decreasing bias voltage. For the bias voltages used in this study, this change is not dramatic as shown by the small variations in OBP. For a fixed bias voltage, the OBP increases with increasing P_{out} and the corresponding OBP varies significantly.
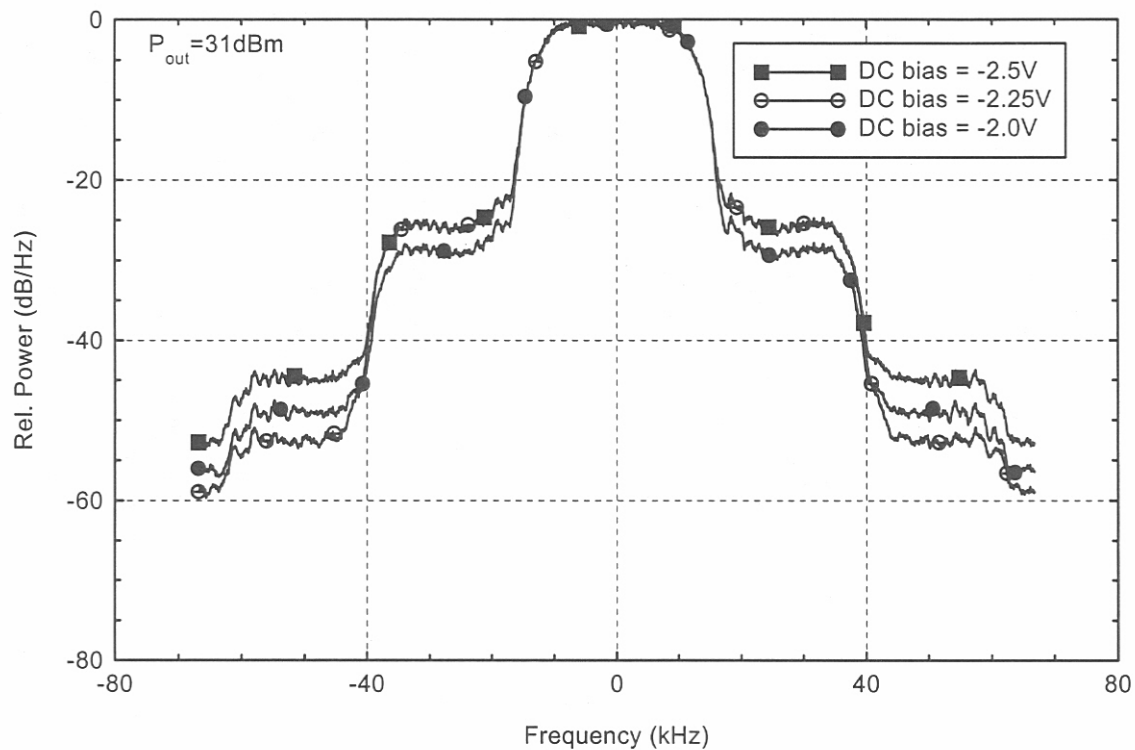
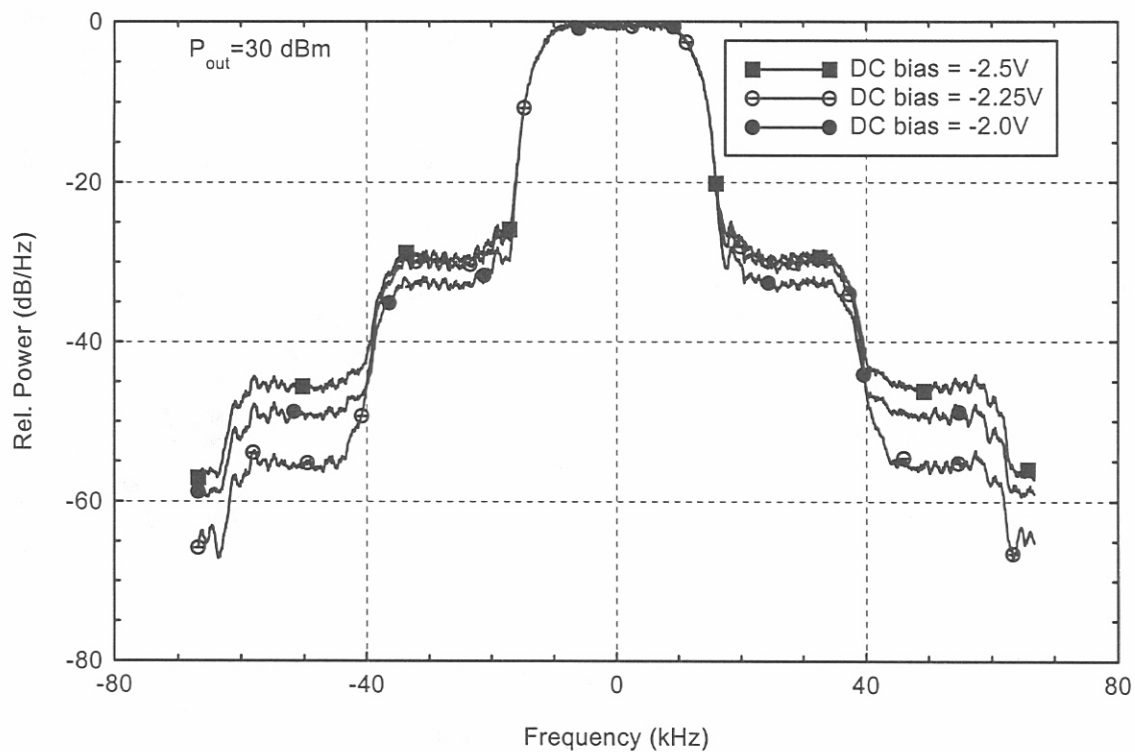Figure 14. PSD at 31 dBm output power for three bias voltages.

Figure 15. PSD at 30 dBm output power for three bias voltages.
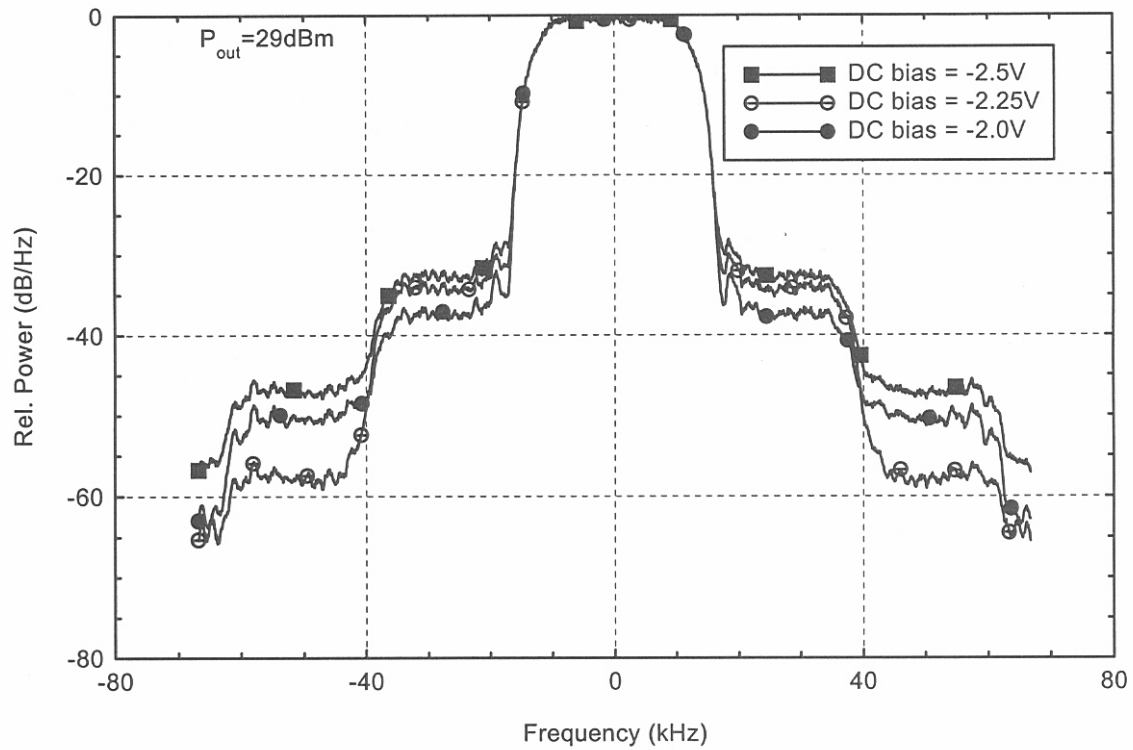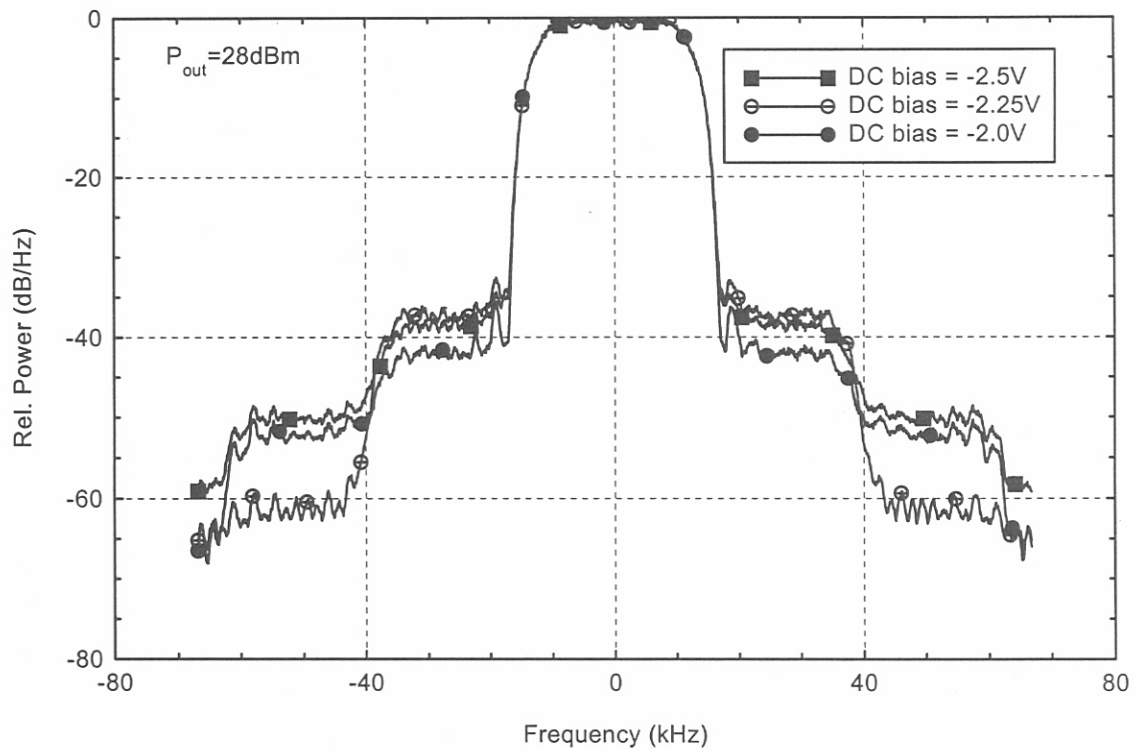
21

Figure 16. PSD at 29 dBm output for three bias voltages.

Figure 17. PSD at 28 dBm output power for three bias voltages.

Table 4. OBP as a Function of Bias Voltage and Output Power

P_{out}	DC bias (V)	OBP (dB)
31 dBm	-2.50	-19.6
	-2.25	-19.6
	-2.00	-21.5
30 dBm	-2.50	-21.9
	-2.25	-22.4
	-2.00	-23.3
29 dBm	-2.50	-23.5
	-2.25	-23.9
	-2.00	-24.6
28 dBm	-2.50	-24.7
	-2.25	-25.2
	-2.00	-25.3

8. RESULTS

For the operating parameters considered in this study, we found that the power amplifier was *most* linear at 28 dBm mean output power and -2.0 V bias. In Table 5 we have summarized the significant results of this study: the relationship between amplifier nonlinearity (a function of bias and output power), the battery current, the OBP, and maximum allowable radio link loss. The tabulated values for OBP and maximum allowable radio link loss are relative to those obtained when the amplifier is operating at -2.0 V bias and 28 dBm mean output power.

The results presented show that the battery current varies by about 20-35% as a function of bias voltage for a fixed output power. Hence, decreasing the bias voltage can have a significant effect on battery current (i.e., talk-time). For the operating parameters under study, the most significant changes in OBP occurred when the output power was reduced. Varying the bias voltage had only a small effect on the OBP when compared to reducing the mean output power by 3 dB. Decreasing battery current by decreasing bias voltage is less effective for the higher output powers. For example,

at 28 dBm, the battery current varied by 360 mA and at 31 dBm it only varied by 190 mA. Thus the results indicate that when operating at the relatively lower output power (i.e., 28 dBm) a significant reduction in battery current is achieved by decreasing the bias voltage with only a small increase in undesirable effects such as OBP and minimal reduction in effective range. At higher input powers, the increase in OBP was somewhat larger and the reduction in current was not as dramatic.

As may be expected, increasing the output power also increased the RLM. The increase in RLM of 2.6 dB is about the same as the 3 dB increase that would be obtained by increasing the output power of a linear amplifier from 28 to 31 dBm.

Table 5. Summary of Results

P_{out}	Bias (V)	Current (mA)	RLM (dB)	Relative OBP (dBc)
31 dBm	-2.50	810	2.6	5.7
	-2.25	1000	2.6	5.7
	-2.00	1000	2.9	3.8
30 dBm	-2.50	740	2.1	3.4
	-2.25	910	2.0	2.9
	-2.00	1000	2.1	2.0
29 dBm	-2.50	710	1.1	2.2
	-2.25	840	1.1	2.6
	-2.00	960	1.0	1.3
28 dBm	-2.50	640	0.1	0.6
	-2.25	800	0.1	0.1
	-2.00	1000	0	0

To the extent that link margins will allow, the most significant reductions in battery current were obtained at lower amplifier output power and bias voltage. For the amplifier under study, a reduction in output signal power of 3 dB at a bias of -2.5 V corresponded to a reduction in RLM of about 2.5 dB, a decrease in OBP of about 5 dB, and a reduction of 170 mA in required battery current (about

a 20% increase in talk-time). Thus if the additional 2.5 dB in RLM is not really necessary for a given system, a definite improvement in both talk-time and spectrum utilization can be obtained by backing off from the maximum rated power for this amplifier.

9. SUMMARY

In this report we have described a measurement, modeling, and simulation effort that analyzed the relationship between battery current, OBP, and link margin for a typical PCS portable transceiver power amplifier. The nonlinear amplifier characteristics and associated battery current were obtained from measurements of the PCS amplifier. The measurements were performed for various amplifier bias voltages and input powers in the range of ±10 dBm. A mathematical model of the power amplifier based on these measurements was used to simulate the communications link in order to determine the PSD and SER for a digitally modulated signal using $\pi/4$ DQPSK with 35% RRC filtering. For this study, the simulations were limited to nonlinear amplifier transfer functions corresponding to bias voltages of -2.0 V, -2.25 V, and -2.5 V; and mean output signal powers of 28, 29, 30, and 31 dBm. The OBP was computed from the simulated PSD's and the SER was used to determine the RLM for a maximum SER of 10^{-3}.

In summary, these results indicate that battery current is strongly dependent on both the bias voltage and the output (or input) power. The results of this study show that power amplifier operating parameters that are selected to improve the quality and convenience of a communication system (e.g., extend battery life and link margin) have a direct consequence in terms of spectrum utilization. Such factors need to be considered in terms of spectrum utilization and allocation when nonlinear amplification of variable envelope modulations are implemented. Although the conclusions are derived from the measurement, modeling, and simulation of a single MMIC power amplifier, the methodology described should be useful for both communication system design and spectrum management. The amplifier studied is used for power amplifying constant and variable envelope modulations in the PCS band. Its main disadvantage, for our purposes, was the inability to control the bias voltage of each of the three amplifier stages. Further work should include this capability. Amplifier operating characteristics such as output power, OBP, and SER can also be controlled via the drain voltage. Such a study was beyond the scope of this effort, but should be considered in future work.

10. REFERENCES

[1] P. Dan, "Make the right battery choice for portables," *Electronic Design,* pp. 115-120, Apr. 1, 1996.

[2] J. Staudinger, "Multiharmonic load termination effects of GaAs MESFET power amplifiers," *Microwave Journal,* pp. 60-77, Apr. 1996.

[3] C. Huang, "GaAs MMIC power amplifiers drive cellular systems," *Microwaves and RF,* pp. 85-86, Oct. 1994.

[4] L. J. Kushner, "Output performance of idealized microwave power amplifiers," *Microwave Journal,* pp. 103-116, Oct. 1989.

[5] L. J. Kushner, "Estimating power amplifier large signal gain," *Microwave Journal,* pp. 87-102, Jun. 1990.

[6] L. Goldberg, "PCS: Technology with fractured standards," *Electronic Design,* pp. 65-78, Feb. 6, 1995.

[7] J. Millman, *Microelectronics,* New York, NY: McGraw Hill, 1979.

[8] S.A. Maas, "MESFET power amplifiers," In ch. 9 of *Nonlinear Microwave Circuits,* Norwood, MA: Artech House, 1988, pp. 359-396.

[9] A.A.M. Saleh, "Frequency-independent and frequency-dependent nonlinear models of TWT amplifiers," *IEEE Trans. Comm.,* vol. COM-29, no. 11, pp. 1715-1720, 1981.

[10] N. Wiener, *Nonlinear Problems in Random Theory,* New York, NY: John Wiley & Sons, Inc., 1958, pp. 28-48.

[11] E. Bedrosian and S. O. Rice, "The output properties of Volterra systems (nonlinear systems with memory) driven by harmonic and Gaussian inputs," *Proceedings of the IEEE,* vol. 59, no. 12, pp. 1688-1707, Dec. 1971.

[12] V. Volterrra, *Theory of Functionals and of Integral and Integro-differential Equations,* New York, NY: Dover Publications, Inc., 1959, pp. 21.

[13] A.V. Oppenheim, *Digital Signal Processing,* Englewood Cliffs, NJ: Prentice Hall Inc., 1975, pp. 553-554.

11. BIBLIOGRAPHY

Power Spectral Density and Adjacent Channel Interference:

J.F. Sevic and J. Staudinger, "Simulation of adjacent-channel power for digital wireless communication systems," *Microwave Journal,* pp. 66-80, Oct. 1996.

S. Aritlyavisitakul and T. Liu, "Characterizing the effects of nonlinear amplifiers on linear modulation for digital portable radio communications," *IEEE Trans. on Veh. Tech.,* pp. 383-389, Nov. 1990.

J. S. Kenney and A. Leke, "Power amplifier spectral regrowth for digital cellular and PCS applications," *Microwave Journal,* pp. 74-92, Oct. 1995.

J.K. Cavers, "The effect of data modulation format on intermodulation power in nonlinear amplifiers," in *Proc. of the 1994 Globecom,* pp. 489-493, 1994.

M. Heutmaker, J.R. Welch, and E. Wu, "Using digital modulation to measure and model RF amplifier distortion," in *Proc. of the Wireless Comm. Conf,* pp. 78-81, Aug. 1996.

GaAs FET modeling:

H. State, P. Newman, I. R. Smith, R. A. Pucel, and H. A. Haus, "GaAs FET device and circuit simulation in SPICE," *IEEE Trans. on Electron Devices,* pp. 160-169, Feb. 1987.

J. Staudinger, M. Golio, C. Woodin, and M. C. deBaca, "Considerations for improving the accuracy of large-signal GaAS MESFET models to predict power amplifier circuit performance," *IEEE Jour. of Solid-State Circuits,* pp. 366-373, Mar. 1994.

R. Howald, "Understanding distortion in GaAs MESFETS," *RF Design,* pp. 71-80, Jun. 1997.

State of the Art Power Amplifiers:

F. A. Olson, "Microwave solid-state power amplifier performance: Present and future," *Microwave Journal,* pp. 24-46, Feb. 1995.

B. Stengel and V. Nair, "RF power amplifiers for portable communications applications," *1994 IEEE MTT-S International Microwave Symposium Digest,* pp. 1623-1626, May 1994.

Improvements:

J. Sheinwald, "MMIC compatible bandpass filter design: A survey of applicable techniques," *Microwave Journal,* pp. 26-42, Mar. 1994.